1992

Experimental Verification of Attitude Control Techniques for Slew Maneuvers of Flexible Spacecraft

Hailey, J.

EXPERIMENTAL VERIFICATION OF ATTITUDE CONTROL TECHNIQUES FOR SLEW MANEUVERS OF FLEXIBLE SPACECRAFT

Jeffrey A. Hailey*, Christopher D. Sortun* and Brij N. Agrawal+
Naval Postgraduate School
Monterey, California 93943-5000

Abstract

This paper presents experimental verification of modern and classical control laws on flexible spacecraft structures. The Flexible Spacecraft Simulator at the Naval Postgraduate School is designed to test a variety of control theory on a two-dimensional representation of an antenna at the end of a low-frequency astromast. The Simulator represents motion about the pitch axis and is restricted to rotatation only. Control laws are implemented through a momentum wheel mounted on the rigid main body. Feedback is obtained through a rotary variable differential transformer (RVDT) which senses the body's rotation angle and a rate-gyro giving body rate. The analytical model contains the linearized equations of motion accounting for the flexible dynamics. Slewing maneuvers are conducted for positioning the main body by using proportional-derivative (PD), torque profiles and optimal controllers. No active control is applied to the flexible structure. A new technique for state estimation is developed for the optimal controller since the standard estimation methods prove to be unsatisfactory. In all cases, the experimental results are in close agreement with the analytical predictions.

Introduction

Analytical techniques for the control of flexible spacecraft structures are rapidly accumulating in the literature while relatively few experiments (References 1, 2, 3) exist for verification. This paper develops a mathematical model of a system exhibiting the low frequency characteristics of a light mass spacecraft structure. The model is developed by using rigid body coordinates for the central body and cantilever modal coordinates for the flexible body. Using this model, classical and modern control theory are applied within the constraints of the experimental hardware. The analytical simulation and experimental results are then compared to examine the accuracy and applicability of the analytical model.

Experimental Setup

The Flexible Spacecraft Simulator configuration is shown in Figure 1. It approximates the pitch axis motion of a spacecraft configuration used in a study conducted by INTELSAT (Reference 4). The Simulator has a central rigid body representing a spacecraft main body and a flexible appendage corresponding to a reflector supported by a flexible astromast. It is floated on a horizontal, smooth granite table to reduce friction and to simulate low-gravity operations in two dimensions since gravity acts perpendicular to all displacements and consequently does no work. The central body is attached to an I-beam above the table through an air-bearing which allows only rotational motion. The assemblage is actuated by a momentum wheel mounted on the main body. A RVDT and a rate-gyro provide the angular position and angular velocity of the central hub, respectively. The fundamental cantilever frequency of the flexible structure is 0.14 Hz.

Control laws are implemented using a VAX station 3100 in conjunction with an AC-100 controller manufactured by Integrated Systems, Inc. The System Build software associated with the AC-100 runs with MATRIXx and allows the user to build control schemes with block diagrams similar to a flow chart. The computer translates these diagrams to C code which is subsequently loaded into the AC-100 for execution. Included in this process is the ability to create custom on-screen displays which allow the user real-time interaction with the controller while it is running. The AC-100 hardware consists of A to D and D to A converters providing many options for sensor and actuator connections.

---

* Lieutenant, United States Navy, Graduate Student
+ Professor, Department of Aeronautics and Astronautics, Associate Fellow

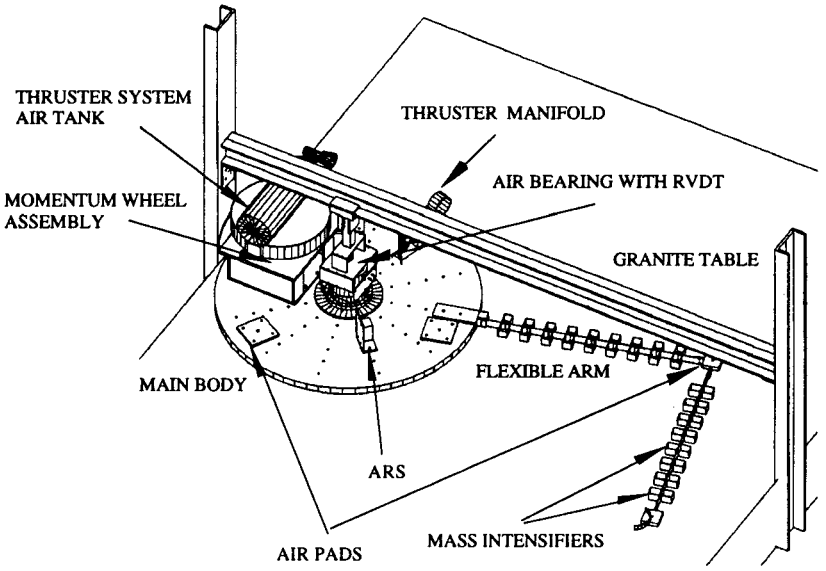

Figure 1. Flexible Spacecraft Simulator Configuration

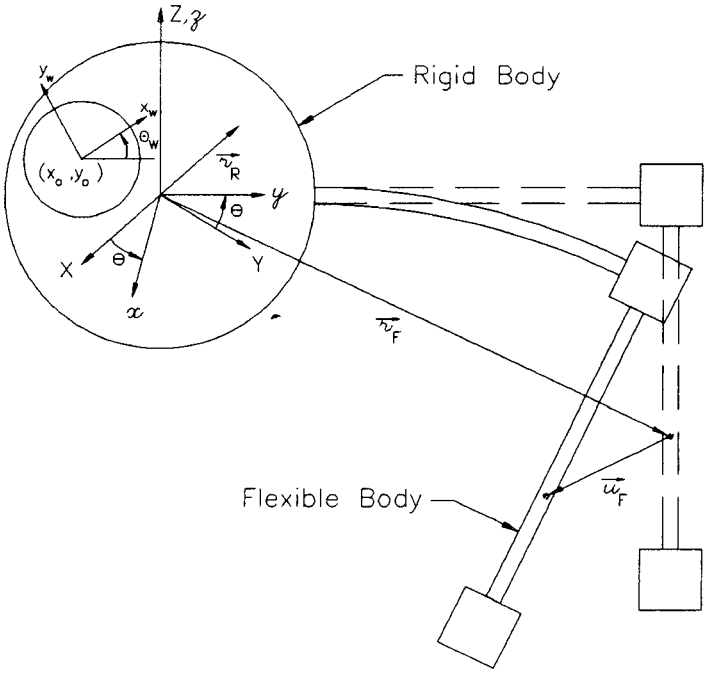

Figure 2. Analytical Model

Analytical Model

The analytical model (Reference 5) is shown in Figure 2. It is comprised of a flexible structure attached to a rigid central body restricted to rotation only. The X, Y, Z axes are inertially fixed. The x, y, z axes are fixed with respect to the rigid body and are obtained through a rotation θ about the Z axis. The x_W, y_W, z_W axes are fixed in the wheel with the origin at point (x_o, y_o, z_o) in the rigid body and are obtained by rotation of θ_W about the z axis. The equations of motion are derived by using a hybrid-coordinate system, rotational angle θ of the rigid body, θ_w of the wheel and cantilever modal coordinates of the flexible body. Lagrange's equations are used and require an expression for the kinetic energy, T.

$$T = \frac{1}{2}\int_R (\vec{V}_R \cdot \vec{V}_R)dm + \frac{1}{2}\int_F (\vec{V}_F \cdot \vec{V}_F)dm + \frac{1}{2}\int_W (\vec{V}_W \cdot \vec{V}_W)dm \quad (1)$$

where $\vec{V}_R$ = velocity of a particle on the rigid body

$\vec{V}_F$ = velocity of a particle on the flexible body

$\vec{V}_W$ = velocity of a particle on the momentum wheel .

The velocities $\vec{V}_R$, $\vec{V}_W$ and $\vec{V}_F$ are given by

$$\vec{V}_R = \dot{\theta}\vec{k} \times \vec{r}_R \quad (2)$$

$$\vec{V}_F = \dot{\theta}\vec{k} \times \vec{r}_F + \dot{\vec{u}} + \dot{\theta}\vec{k} \times \vec{u} \quad (3)$$

$$\vec{V}_W = (\dot{\theta} + \dot{\theta}_W)\vec{k} \times \vec{r}_W + \dot{\theta}\vec{k} \times \vec{r}_o \quad (4)$$

where $\vec{r}_R$ = position vector of a particle on the rigid body

$\vec{r}_F$ = position vector of a particle on the flexible body

$\vec{r}_W$ = position vector of a particle on the momentum wheel

$\vec{u}$ = elastic deformation vector of a particle on the flexible body

k = unit vector along the z axis

Substituting Equations (2) and (3) into Equation (1) yields

$$\begin{aligned} T = {} & \frac{1}{2}\int_R \dot{\theta}^2 (x_R^2 + y_R^2)dm \\ & + \frac{1}{2}\int_F \left[\dot{\theta}^2 (x_F^2 + y_F^2) + (\dot{u}_x^2 + \dot{u}_y^2) + \dot{\theta}^2 (u_x^2 + u_y^2)\right]dm \\ & + \frac{1}{2}\int_F \left[2\dot{\theta}(x_F\dot{u}_y - y_F\dot{u}_x) + 2\dot{\theta}^2 (x_F u_x + y_F u_y)\right]dm \\ & + \int_F \left[\dot{\theta}(\dot{u}_y u_x - \dot{u}_x u_y)\right]dm \quad (5) \\ & + \frac{1}{2}\int_W \left[\dot{\theta}^2 (x_o^2 + y_o^2) + \dot{\theta}^2 (x_W^2 + y_W^2)\right]dm \\ & + \frac{1}{2}\int_w \left[2\dot{\theta}^2 (x_o x_W + y_o y_W) + \dot{\theta}_W^2 (x_W^2 + y_W^2)\right]dm \\ & + \frac{1}{2}\int_W \left[2\dot{\theta}\dot{\theta}_W (x_W^2 + y_W^2) + 2\dot{\theta}_W\dot{\theta}(x_o x_W + y_o y_W)\right]dm \end{aligned}$$

The generalized coordinates used for the equations of motion will be θ, θ_W, and u. Assuming the wheel is rotating about its center of mass eliminates terms with single powers of x_W and y_W. After linearizing about assumed small displacements and rates, we get

$$\begin{aligned} T = {} & \frac{1}{2} I_{ZZ}\dot{\theta}^2 + \frac{1}{2} I_W \dot{\theta}_W^2 + I_W \dot{\theta}\dot{\theta}_W \\ & + \frac{1}{2}\int_F (\dot{u}_x^2 + \dot{u}_y^2)dm \quad (6) \\ & + \dot{\theta}\int_F (x_F\dot{u}_y - y_F\dot{u}_x)dm \end{aligned}$$

where

$$I_{ZZ} = I_{ZZ}^R + I_{ZZ}^F + I_{ZZ}^W$$
$$= \int_R (x_R^2 + y_R^2)dm + \int_F (x_F^2 + y_F^2)dm$$
$$+ \int_W (x_W^2 + y_W^2)dm + m_W(x_O^2 + y_O^2) \quad (7)$$

The elastic deformation u is represented in terms of cantilever modal coordinates of the flexible body as

$$u_x = \sum_{i=1}^{n} \phi_i^x q_i(t)$$
$$u_y = \sum_{i=1}^{n} \phi_i^y q_i(t) \quad (8)$$

where for the i_{th} mode, $q_i(t)$ is the modal coordinate, ϕ_i^x is the component of the modal vector along the x axis, and ϕ_i^y is the component of the modal vector along the y axis. Substituting Equation (8) into Equation (6) gives

$$T = \frac{1}{2} I_{ZZ} \dot{\theta}^2 + \frac{1}{2} I_W \dot{\theta}_W^2 + I_W \dot{\theta} \dot{\theta}_W$$
$$+ \frac{1}{2} \int_F \left(\sum_{i=1}^{n} \sum_{j=1}^{n} \left[\phi_i^x \phi_j^x + \phi_i^y \phi_j^y \right] \dot{q}_i \dot{q}_j \right) dm$$
$$+ \dot{\theta} \int_F \left[x_F \sum_{i=1}^{n} \phi_i^y \dot{q}_i - y_F \sum_{i=1}^{n} \phi_i^x \dot{q}_i \right] dm \quad (9)$$

Normalizing the modal vectors to unity modal masses (mass normalizing) and using orthogonality of the modal vectors, Equation (9) is simplified to

$$T = \frac{1}{2} I_{ZZ} \dot{\theta}^2 + \frac{1}{2} I_W \dot{\theta}_W^2 + I_W \dot{\theta} \dot{\theta}_W + \frac{1}{2} \sum_{i=1}^{n} \dot{q}_i^2$$
$$+ \dot{\theta} \sum_{i=1}^{n} D_i \dot{q}_i \quad (10)$$

where

$$D_i = \int_F (x_F \phi_i^y - y_F \phi_i^x) dm$$

= rigid elastic coupling.

The potential energy of the flexible body due to elastic stiffness in terms of modal coordinates is given by

$$V = \frac{1}{2} \sum_{i=1}^{n} \omega_i^2 q_i^2 \quad (11)$$

where ω_i is the is the natural frequency of the i_{th} mode.

The Lagrange's equation is

$$\frac{d}{dt}\left(\frac{\partial L}{\partial \dot{\mu}_i}\right) - \frac{\partial L}{\partial \mu_i} = Q_i \quad (12)$$

where L = T - V, μ_i is the generalized coordinate and Q_i is the generalized force. The generalized coordinates for the system are θ, θ_W, q_i, ..., q_n. Let T_C be the torque acting between the momentum wheel and the rigid body and T_D be the external torque acting on the central body. The virtual work done by these torques is

$$\delta W = -T_c \delta(\theta - \theta_W) + T_c \delta\theta + T_D \delta\theta$$
$$= -T_c \delta\theta_W + T_D \delta\theta \quad (13)$$

Therefore,

$$Q_\theta = T_D$$
$$Q_{\theta W} = -T_c \quad (14)$$

Substituting Equations (10), (11) and (13) into Equation (12), the equations of motion of the system are

$$I_{ZZ} \ddot{\theta} + \sum_{i=1}^{n} D_i \ddot{q}_i + I_W \ddot{\theta}_W = T_D$$
$$\ddot{q}_i + \omega_i^2 q_i + D_i \ddot{\theta} = 0$$
$$I_W \ddot{\theta}_W = I_W \dot{\Omega} = -T_c \quad (15)$$

where

$\dot{\Omega}$ = spin rate of the wheel with respect to the central body

Assuming modal damping for the cantilever modes, the equations of motion become

$$I_{zz}\ddot{\theta} + \sum_{i=1}^{n} D_i\ddot{q}_i = T_t = T_D + T_c$$

$$\ddot{q}_i + 2\xi_i\omega_i\dot{q}_i + \omega_i^2 q_i + D_i\ddot{\theta} = 0 \qquad (16)$$

A state space representation of the system equations is

$$\dot{X} = [A]X + [B]U$$
$$Y = [C]X + [D]U \qquad (16)$$

where $X = \left[\theta, q_1, \cdots, q_n, \dot{\theta}, \dot{q}_1, \cdots, \dot{q}_N\right]^T$

$$Y = \left[\theta, \dot{\theta}\right]^T$$

$$U = T_t \qquad (17)$$

$$D = 0$$

$$A = \begin{bmatrix} 0 & 0 & \cdots & 0 & I_{zz}^0 & 0 & \cdots & 0 \\ 0 & 0 & \cdots & 0 & 0 & I_{zz}^0 & \cdots & 0 \\ \vdots & \vdots & & \vdots & \vdots & \vdots & & \vdots \\ \frac{1}{I_{zz}^0} & F_1 & \cdots & F_n & 0 & H_1 & \cdots & H_n \\ 0 & -G_1 & \cdots & -D_iF_n & 0 & J_1 & \cdots & D_1H_n \\ \vdots & \vdots & & \vdots & \vdots & \vdots & & \vdots \\ 0 & -D_nF_1 & \cdots & -G_n & 0 & -D_nH & \cdots & -J_n \end{bmatrix}$$

where

$$I_{zz}^0 = I_{zz} - \sum_{i=1}^{n} (D_i)^2$$

$$F_i = D_i\omega_i^2$$

$$G_i = \omega_i^2 I_{zz}^0 + D_iF_i \qquad (18)$$

$$H_i = 2\xi_i\omega_iD_i$$

$$J_i = 2\xi_i\omega_iI_{zz}^0 + D_iH_i$$

$$[C] = \begin{bmatrix} 1 & 0 & \cdots & 0 & 0 & 0 & \cdots & 0 \\ 0 & 0 & \cdots & 0 & 1 & 0 & \cdots & 0 \end{bmatrix} \qquad (19)$$

Proportional - Derivative Control

Analytical simulations were performed using the first six cantilever modes of the flexible appendage. The modal characteristics, natural frequencies and mode shapes are determined using the GIFTS finite element analysis program. For all the modes, modal damping has been experimentally determined to be 0.4 percent critical damping. Strain gauges are used to evaluate the modal damping. This causes X in Equation (16) to be a 14 state vector.

The classical technique of proportional derivative control is used by feeding back the central body angular position and angular rate. The control torque T_c is given by

$$T_c = -k(\theta_e + \tau\dot{\theta}) \qquad (20)$$

where θ_e = angular error of the rigid body

$= \theta - \theta_{ref}$

$\dot{\theta}$ = angular rate of the body

k = gain for the control

τ = time constant

The equation for the reaction wheel is

$$I_W\dot{\Omega} = -T_c \qquad (21)$$

A variable cable induced spring torque affects the nominal angular position of the experimental setup. Assuming this torque to be constant during the maneuver,

$$T_t = -k(\theta_e + \tau\dot{\theta}) + T_D \qquad (22)$$

The analytical simulation and experimental results are plotted together in Figure 3 for a 60° slew. The dashed lines represent experimental data and the solid lines represent analytical prediction. There is a steady state error given by

$$\theta_{ss} = \frac{T_D}{k} \qquad (23)$$

The control gains are determined with the classical pole placement analysis for a rigid body. The control bandwidth is limited to half the fundamental frequency of the flexible appendage and the damping ratio is set to 0.9. The classical characteristic equation for the rigid $\frac{1}{s^2}$ plant is

$$s^2 + 2\xi\omega_n s + \omega_n^2 = 0 \qquad (24)$$

ω_n = controller natural frequency = 0.06 Hz

ξ = damping ratio

From this the poles of the rigid system can be determined leading to the rigid body gains using $MATRIX_x$.

k = 1.3985 N-m/rad

$k\tau$ = 6.6773 N-m-s/rad .

The steady state position error is caused by a spring torque in the cabling to the motor. The cable spring torque is evaluated by observing the reaction wheel speed change after the assemblage has reached a steady state. The experimental steady state position error can be used to check the spring torque calculation with Equation (23). Figure 4 is the analytical arm deflection over time for a 60° slew. Figure 4 also shows the arm motion with the base point location adjusted for better comparison.

Figure 3 shows a substantial control effort when the controller is turned on. This equates to an initial impulse followed by compensating control torques which is undesirable since the initial torque causes large fluctuations in the flexible appendage. The PD controller is also in contradiction to our linear assumptions of small displacements and rates. These points will be addressed in a later section.

Torque Shaping -- Pseudo-Square

Efforts to apply the classic Bang-Bang control law to the Flexible Spacecraft Simulator were mostly unsuccessful. Two reasons for its incompatibility are readily apparent and can be addressed using torque shaping techniques. First, when applied to the flexible model, the Bang-Bang controller switches frequently. This causes many discontinuities resulting in the chattering evident from previous results. Second, the rise time associated with the maneuver cannot be realized by the reaction wheel. Reference 2 describes a scheme for conducting near minimum time maneuvers by rounding off the corners of the Bang-Bang square wave torque and following this modified profile. This gives the wheel time to respond to the commanded torque assuming a realistic rise time is set. The resulting maneuver is a near-minimum-time slew which does not over-excite the flexible modes.

The torque shaping is accomplished by combining sections of a sine wave with horizontal line sections. The sine function has a period of four times the specified rise time. The general control law is

$$u = -u_{max}\, f(t_r, t, P) = I_{zz}^0 \ddot{\theta} \qquad (25)$$

where u_{max} = maximum desired torque level

t_r = specified rise time

The function $f(t_r,t,P)$ is given by

$$f = \begin{Bmatrix} \sin\frac{\pi t}{2t_r} & 0 \le t \le t_r \\ 1 & t_r \le t \le \frac{P}{2} - t_r \\ \sin\frac{\pi\left(t - \frac{P}{2} - 2t_r\right)}{2t_r} & \frac{P}{2} - t_r \le t \le \frac{P}{2} + t_r \\ -1 & \frac{P}{2} + t_r \le t \le P - t_r \\ \sin\frac{\pi(t - P + 4t_r)}{2t_r} & P - t_r \le t \le P \end{Bmatrix} \qquad (26)$$

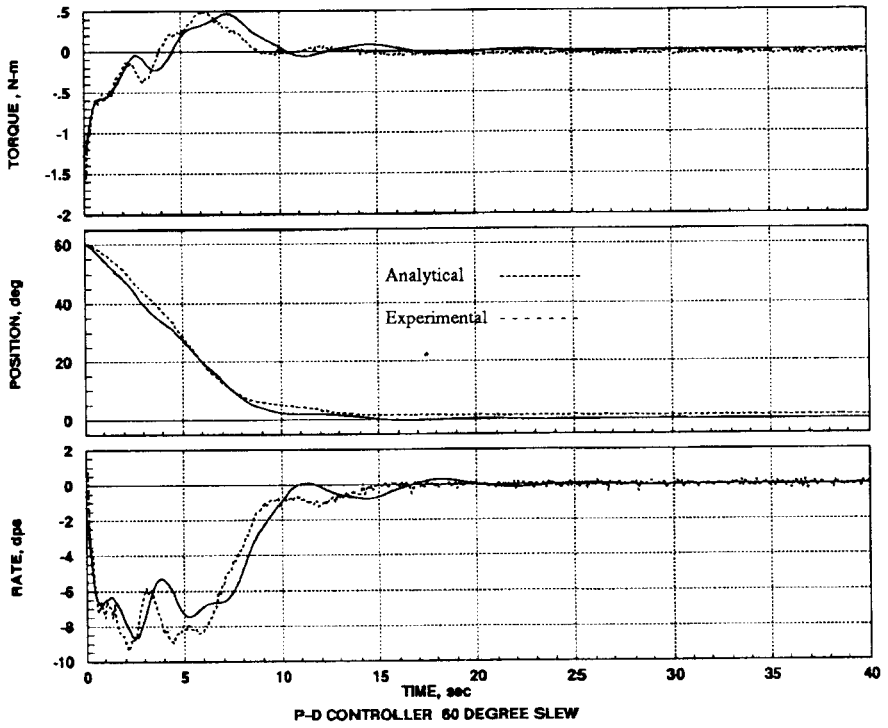

Figure 3. PD Controller Response

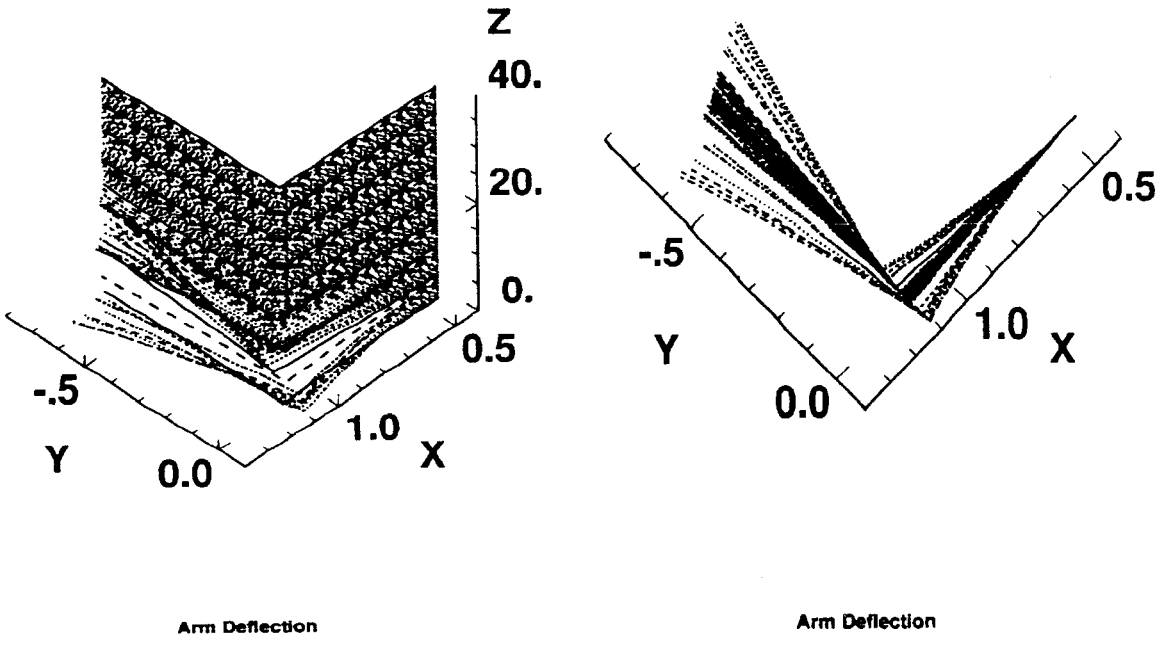

Figure 4. Arm Deflection for a 60° Slew

The resulting torque model is shown in Figure 5 for a 60° slew. Successive integration yields the angular position and angular rate reference curves also in Figure 5. Applying these as references for the flexible assemblage and using the same feedback gains determined for the PD controller gives the results shown in Figure 6 for a 60° slew.

By following position and rate trajectories, the control system is able to accomplish the slew maneuver without inducing severe transients to the momentum wheel. Also, the controller does not chatter or switch frequently. The actual torque path followed is significantly smoother than the modeled torque because the feedback gains are small..

Torque Shaping -- Sinusoidal

A sinusoidal torque profile was also analyzed. It is given by

$$T_c = A\sin\frac{2\pi t}{P} \tag{27}$$

where A = Peak amplitude of the control effort

P = Desired slew time (period of the sinusoid)

The control torque relates to the wheel and body torques as

$$-I_W\dot{\Omega} = -T_c = I_{zz}^0\ddot{\theta} \tag{28}$$

and the feedback control law is

$$u = -k(\theta_e + \tau\dot{\theta}_e) \tag{29}$$

$$\theta_e = \theta - \theta_{ref}$$

$$\dot{\theta}_e = \dot{\theta} - \dot{\theta}_{ref}$$

The reference curves must be in terms of the body position and rate since these are the only states being sensed. They are derived by putting Equation (28) in terms of the body's acceleration and performing successive integrations.

$$\ddot{\theta} = -\frac{A}{I_{zz}^0}\sin\frac{2\pi t}{P} \tag{30}$$

$$\dot{\theta} = \frac{AP}{2\pi I_{zz}^0}\left[\cos\frac{2\pi t}{P} - 1\right] \tag{31}$$

$$\theta = \frac{AP}{2\pi I_{zz}^0}\left[\frac{P}{2\pi}\sin\frac{2\pi t}{P} - t\right] \tag{32}$$

Applying the boundary conditions $\theta = \Delta\theta$ at t=0 and $\theta = 0$ at t=10 for a ten second slewing time and differentiating successively, the reference position and rate are

$$\theta_{ref} = \Delta\theta\left[1 + \frac{1}{P}\left(\frac{P}{2\pi}\sin\frac{2\pi t}{P} - t\right)\right] \tag{33}$$

$$\dot{\theta}_{ref} = \frac{\Delta\theta}{P}\left[\cos\frac{2\pi t}{P} - 1\right] \tag{34}$$

where $\Delta\theta$ = Difference between current and desired position

The body acceleration is given by

$$\ddot{\theta}_{ref} = -\frac{2\pi\Delta\theta}{P^2}\sin\frac{2\pi t}{P} = -\frac{A}{I_{zz}^0}\sin\frac{2\pi t}{P} \tag{35}$$

The reference curves are shown in Figure 7. By manipulating Equation (35), we can examine the tradeoffs between control effort and slewing time with respect to slew angle. The amplitude of the control effort is

$$A = \frac{2\pi I_{zz}^0\Delta\theta}{P^2} \tag{36}$$

and the slew time is given by

$$P = \sqrt{\frac{2\pi\Delta\theta}{A}} \tag{37}$$

By pre-determining the shape and amplitude of the control effort, the slew time required for a rigid body can be determined. By implementing these reference curves into our flexible model, an analytical prediction can be developed to approximate the ensuing motion. Figure 8 compares the predicted motion and the experimental results using the same gains determined in the PD control law during a 60° slew.

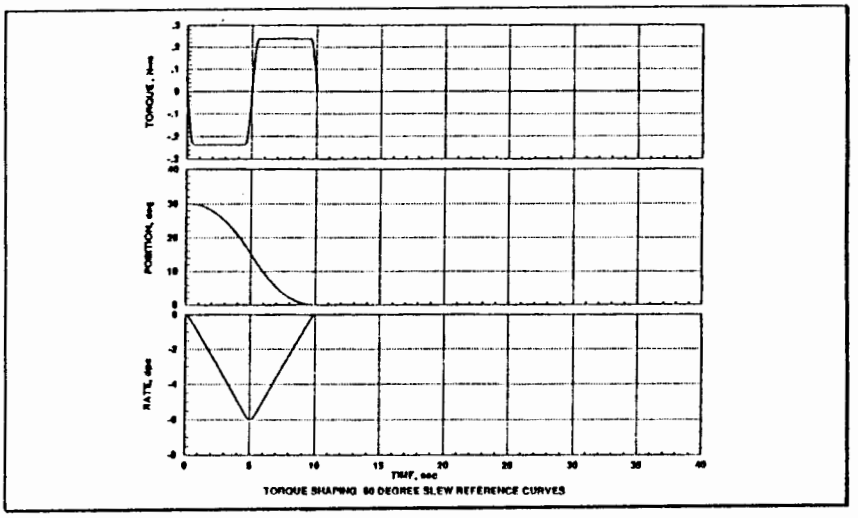

Figure 5. Pseudo-Square Reference Curves

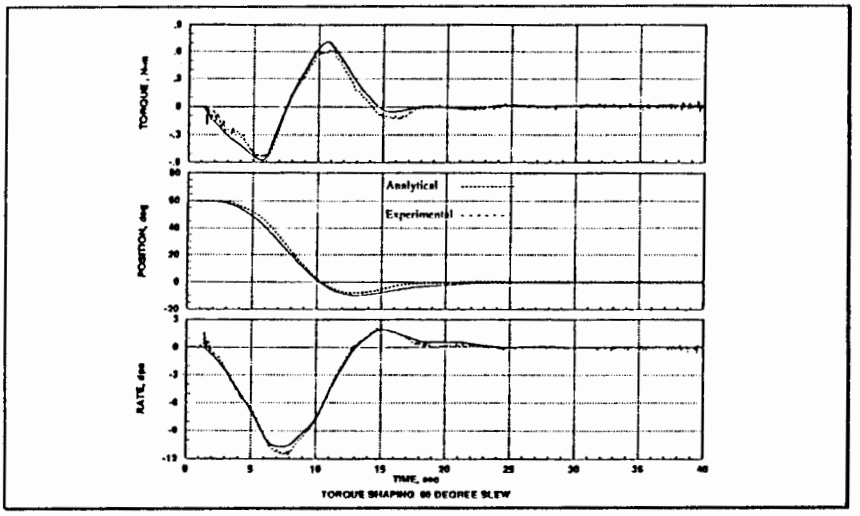

Figure 6. Pseudo-Square Controller Response

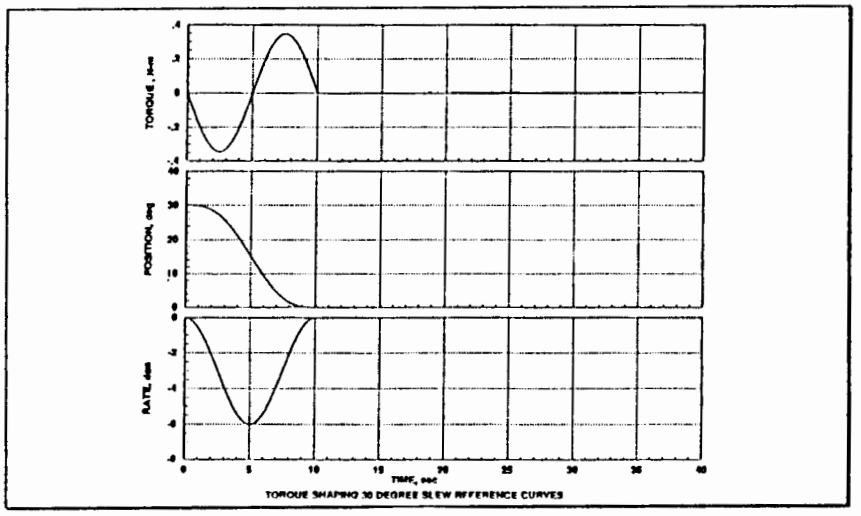

Figure 7. Sinusoidal. Reference Curves

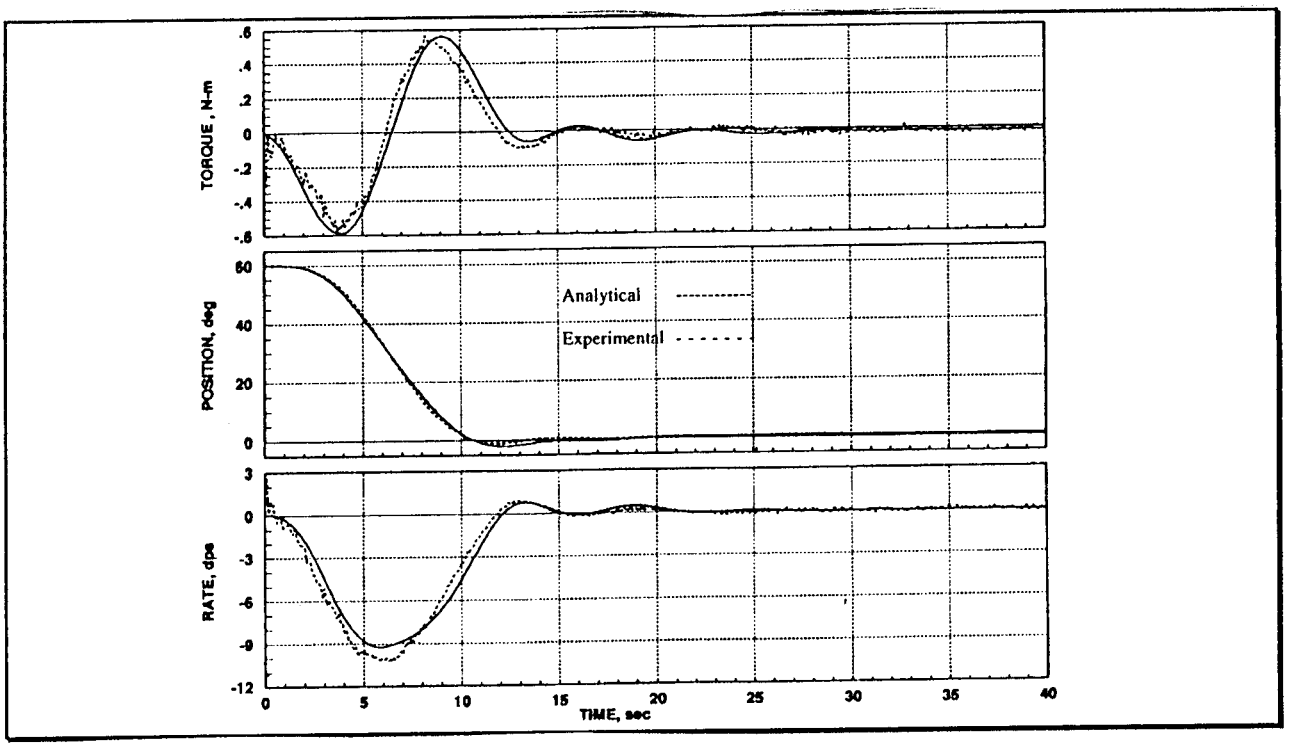

Figure 8. Sinusoidal Torque Shape Response

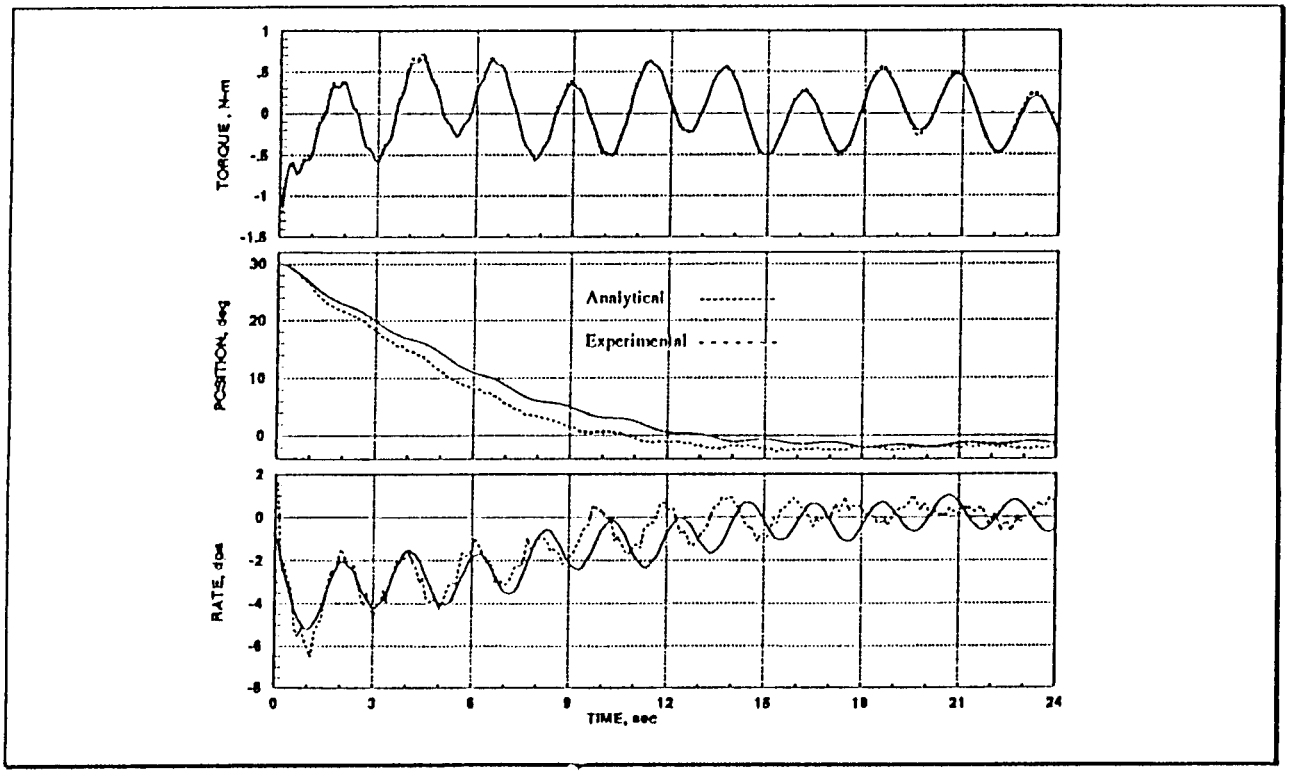

Figure 9. LQG Response

Optimal Control

Using rigid body gains in the feedback control loop is too basic and does not produce the optimum slew maneuver. The ultimate goal in our research is to slew as quickly as possible while suppressing the flexible motion as much as possible. By using a linear-quadratic-gaussian (LQG) compensator we can determine feedback gains based on the rigid and flexible dynamics of the system. The LQG compensator is composed of a linear regulator and a Kalman filter estimator making the estimator more robust in the presence of sensor noise. The regulator design assumes full-state feedback. Feeding back all of the states should yield an improvement over classical PD control. The optimal gains are calculated by minimizing the cost function (Reference 6)

$$\text{cost} = \int_0^\infty \left(x^T R_{xx} x + u^T R_{uu} u\right) dt \tag{38}$$

where R_{xx} is the state weighting matrix and R_{uu} is the input weighting matrix. To determine the gains, we must first solve the Ricatti equation for $\overline{P}$

$$0 = \overline{P}A + A^T\overline{P} - \overline{P}BR_{uu}^{-1}B^T\overline{P} + R_{xx} \tag{39}$$

where A and B are the system dynamic and control input matrices. The optimal regulator gain is

$$K_R = R_{uu}^{-1}B^T\overline{P} \tag{40}$$

The Kalman filter gains are determined in a similar manner using the duality principle. The state and input weighting matrices, R_{xx} and R_{uu}, are replaced by the state and observation noise intensities, Q_{xx} and Q_{yy}. The linear time-invariant system is

$$\begin{aligned} \dot{x} &= Ax + Bu + Fw \\ y &= Cx + Du + \nu \end{aligned} \tag{41}$$

where F = the input disturbance matrix

w = the input disturbance

ν = the measurement noise

The observation noise intensities are related by

$$\begin{aligned} E\left(\nu(t)\nu^T(\tau)\right) &= Q_{yy}\delta(t - \tau) \\ E\left(Fw(t)\nu^T(\tau)\right) &= Q_{xy}\delta(t - \tau) \end{aligned} \tag{42}$$

where E is the expected value operator and δ is the delta function. The system is assumed to be driven by only white noise with zero mean value. A random disturbance of 0.1 N-m amplitude is assumed so that

$$Q_{xx} = B(0.1)B^T \tag{43}$$

Q_{yy} is a 2X2 matrix with diagonal elements corresponding to noise from the RVDT and the angular rate sensor respectively. These have been experimentally determined as

$$Q_{yy} = \begin{bmatrix} 1E\text{-}7 & 0 \\ 0 & 5E\text{-}6 \end{bmatrix} \tag{44}$$

The off-diagonal elements represent cross-correlation of the sensors noises which are assumed to be zero.

The Kalman filter gains are computed by again solving the Ricatti equation (Equation 39) and applying Equation (40). The gains are now represented in a 14X2 matrix since the inputs to the Kalman filter are the two sensed states, angular position and angular rate.

The estimator is now synthesized using the A, B and C matrices of the dynamic system and the estimator gain, K_E.

$$SOBS = \left[\begin{array}{c|c|c|c} A - K_E C & -B & K_E \\ \hline C & 0 & 0 \end{array}\right] \tag{45}$$

where SOBS is the estimator system matrix. The estimated states are then fed to the regulator and result in a commanded torque.

To obtain numerical values for the estimator and regulator gains, the input and state weighting matrices must be determined. R_{xx} is a 14X14 diagonal matrix assuming that none of the states are cross-correlated. Each term on the diagonal corresponds to a state. The body position and body rate (states 1 and 8) are of primary importance and receive a value of one. The first and second modal coordinates and rates (states 2,3,9 and 10) are also of interest and receive weights of 0.5. The remainder of the states are weighted at 0.1. R_{uu} is a scalar since torque is the only system input and is set at 7 in order to prevent excessive oscillations. Figure 9 shows the analytical and experimental results for a 30° slew. The torque prediction is nearly perfect while the position and rate respond faster than predicted. Figure 10 shows the reconstructed position states versus the modeled states. The trouble with the controller's performance obviously lies in the state estimation.

Estimator Refinement

Most of the modern control schemes require full state feedback. Normally this does not present much of a problem since estimated states can be derived from available sensor information. With the Flexible Spacecraft Simulator, however, none of the flexible modes are available.

Both of the dynamic models are derived from rigid body motion combined with flexible vibration. The fourteen states contain the rigid body position and rate as well as the six flexible displacements and velocities. These raw states are mapped into different spaces for each model using modal matrices. Of the fourteen states, only two are available for direct feedback. The other twelve must be estimated by some means for the controllers which require full state feedback. No direct modal information is available since the two sensed states are the rigid body ones. Consequently, the only information available about the flexible motion is contained in the analytical model which is known to be imperfect.

The most obvious method to construct the states is the Kalman estimator. The results of using this method are given in the previous section which proves it to be inadequate for real time control. Applying loop transfer recovery only improves the rigid body state reconstruction. Another approach is to use the Kalman estimator with a smarter choice of weighting matrices. The Kalman state equation is

$$\dot{\hat{\underline{x}}} = (A + BG)\hat{\underline{x}} + KC\underline{e} \tag{46}$$

where $\underline{x}$ = true states

$$\hat{\underline{x}} = \text{estimated states} = \underline{x} + \underline{e} \tag{47}$$

The system dynamics are

$$\begin{aligned} \dot{\underline{x}} &= A\,\underline{x} + B\,\underline{u} \\ \underline{u} &= G\,\hat{\underline{x}} = G\,\underline{x} + G\,\underline{e} \end{aligned} \tag{48}$$

Substituting Equations (46) and (48) into the derivative of Equation (47) gives

$$\dot{\underline{e}} = (A + KC)\underline{e} \tag{49}$$

This is the basis of the Separation Principle which allows one to build the Optimal Regulator by assuming that full state feedback is already available. In effect, the estimator and the regulator are built separately and without knowledge of each other. However, Equation (48) can be written as

$$\dot{\underline{x}} = (A + BG)\,\underline{x} + BG\,\underline{e} \tag{50}$$

This says that the "actual" system dynamics are perturbed by the estimation error, $\underline{e}$. This perturbation is compounded by the REGULATOR gains, G, which leads to a curious conclusion. Although the regulator and the estimator may be considered separately, the dynamics of the system are altered by the regulator gains acting on the estimation error. To build an estimator that will best return the "actual" dynamics, one might minimize the second term in Equation (50) using a linear quadratic approach

$$J = \int \underline{e}^T G^T B^T B G \underline{e}\, dt \tag{51}$$

A weighting matrix can be identified from Equation (51) that corresponds to the Q_{XX} matrix used in the $Matrix_X$ version of the Riccati equation solver. Q_{XX} is the state noise intensity. From Equation (51)

$$Q_{xx} = G^T B^T B G \tag{52}$$

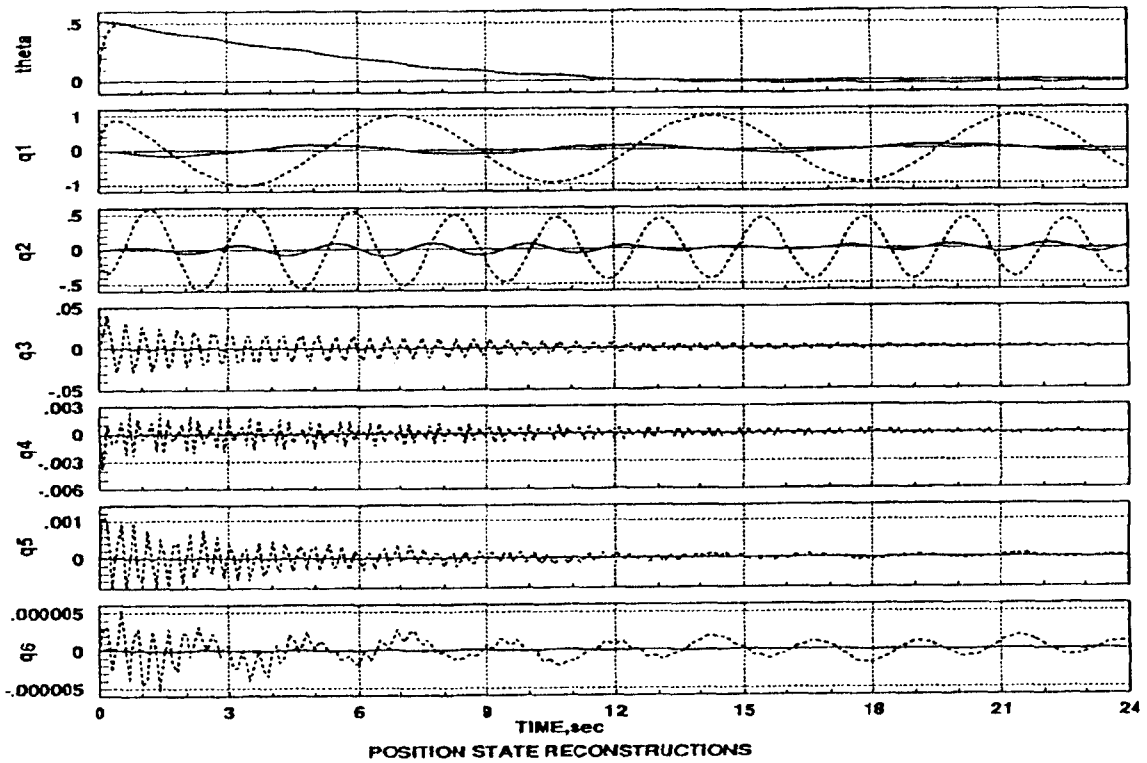

Figure 10. Reconstructed States / First Attempt

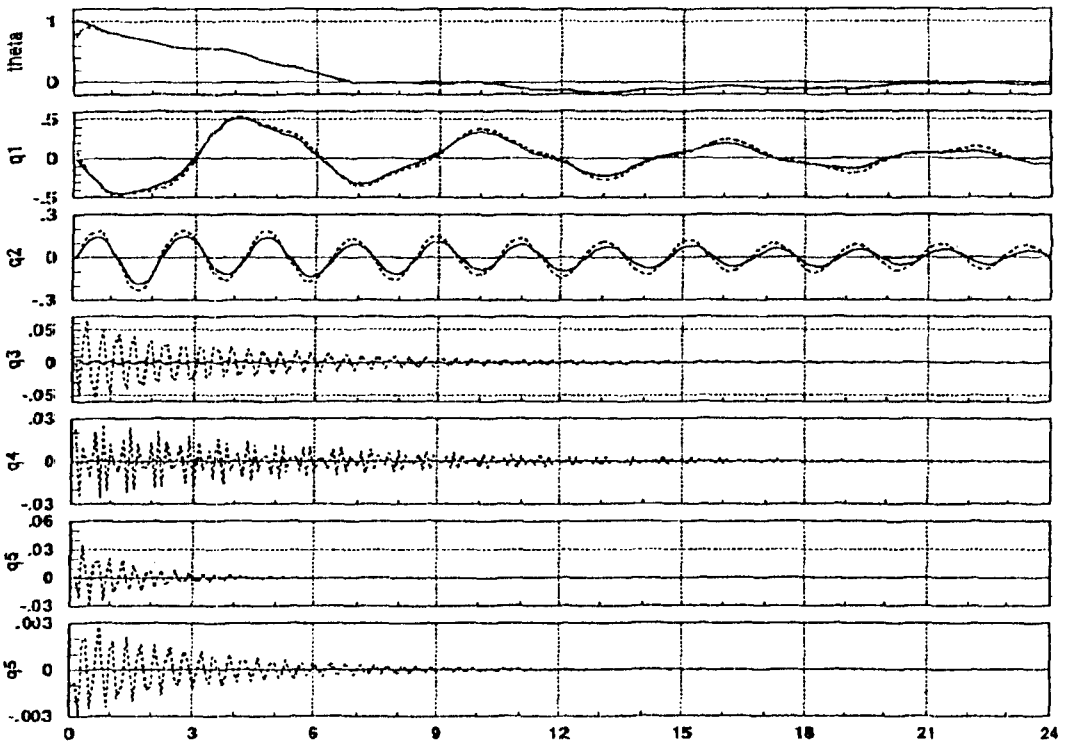

Figure 11. Reconstructed States / Second Attempt

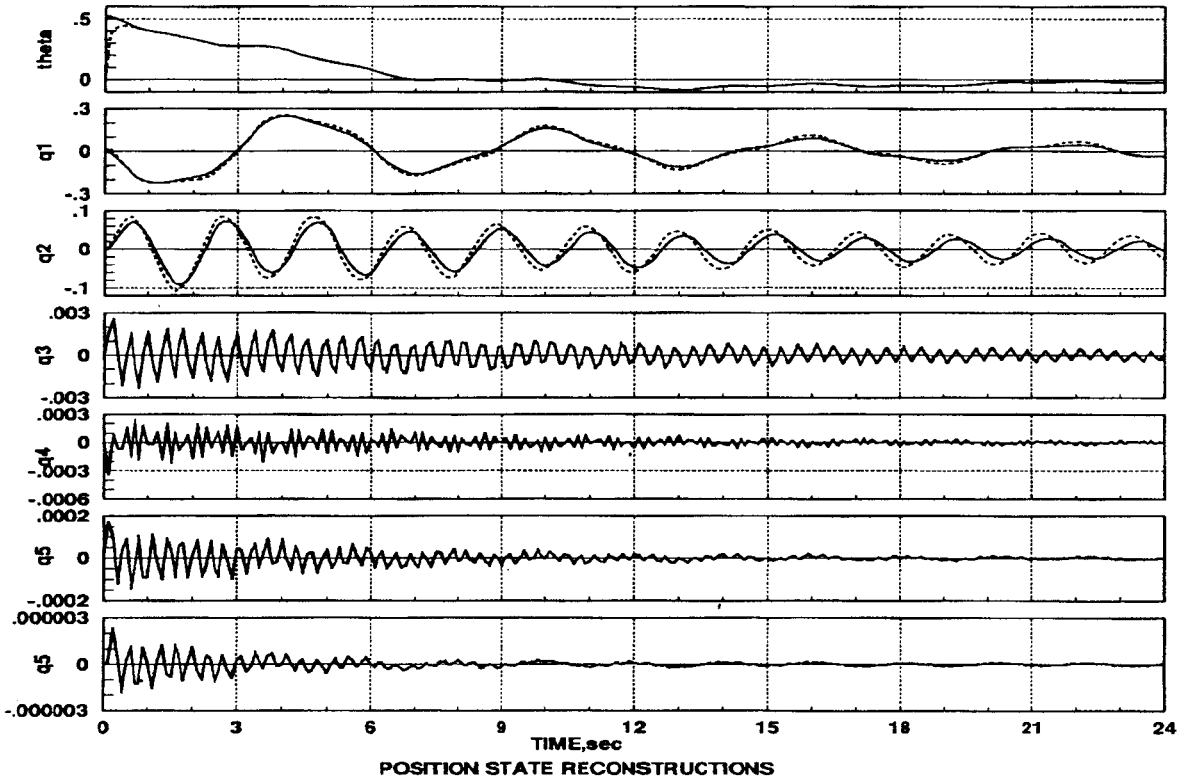

Figure 12. Improved Reconstructed States

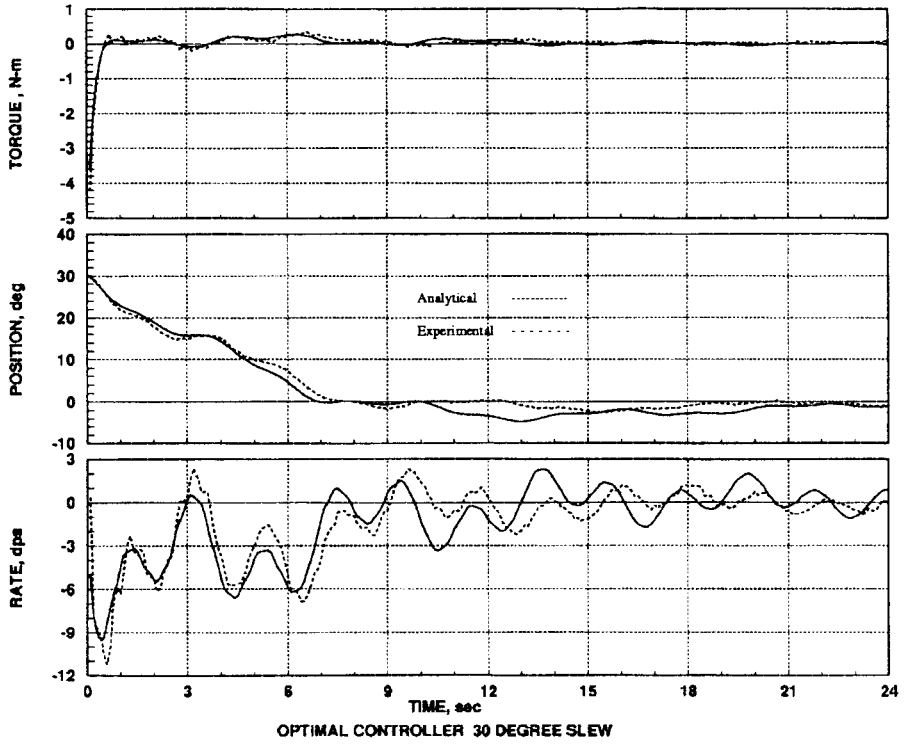

Figure 13. Optimal Controller Response

The results of using Equation (52) in the Kalman estimator are shown in Figures 11. There is considerable improvement in the reconstruction of the first two flexible modes over those in Figure 10.

Looking at Figure 11. one can see that the last four modes have time constants that will play havoc on the dynamic system when fed back. If the regulator is modified so that the gains corresponding to these states are set to zero, the feedback controller will be reduced from 14^{th} order to 6^{th} order.

$$= [\, g1\ g2\ g3\ 0\ 0\ 0\ 0\ g8\ g9\ g10\ 0\ 0\ 0\ 0] \qquad (53)$$

Substituting the new 6^{th} order regulator gains (Equation 53) into Equation (52) and recalculating the estimator gains yields the estimated states shown in Figure 12. In effect, this procedure gives the closed loop estimation for states corresponding to the first three modes and the open loop estimation for the rest of the states. The sensor noise weighting matrix Qyy remains the same as in the previous section. The analytical and experimental results for a 30° slew are shown in Figure 13. Comparing these results to Figure 11, one can see a significant improvement.

Conclusions

Experimental results obtained on the Flexible Spacecraft Simulator are in good agreement with analytical predictions based on the linearized model of the system. Several slewing techniques were explored with the best results coming from the torque shaping scheme. Rigid body gains were used throughout but optimal gains theoretically can be used to achieve faster slewing times while suppressing oscillations. Preliminary research has begun to determine the optimum state and input weightings for the linear-quadratic-gaussian controller. Efforts to build a more effective compensator continue and further results will be included in the final draft of this paper.

Further Research

The experimental setup will be expanded to include piezoelectric sensors and actuators, thrusters, robotics and liquid slosh/control. Piezoelectric devices were used to determine damping in the flexible appendage and preliminary research has begun to use them as actuators for increased damping during a slew maneuver. Thrusters will be used for investigation of flexible interactions during wheel desaturation and for actuating slew maneuvers in place of the momentum wheel. Motors will be attached to the shoulder, elbow and endpoint of the arm for experiments in space robotics. Finally, liquid tanks will be added on the central body to study liquid slosh/control interactions.

Acknowledgements

The authors would like to acknowledge the significant contributions of LT. R.J. Watkins, LT. E.S. Jones and Mr. R. Bailey in making the experimental setup operational.

References

Juang, Jer-Nan, Horta, L.G., and Robert Shaw, H.H., "A Slewing Control Experiment for Flexible Structures," Journal of Guidance, Control and

Dynamics, Vol. 9, NO. 5, Sept.-Oct., 1986, PP. 599-607.

Junkins, J., Rahman, Z., and Bang, H., "Near-Minimum-Time Maneuvers of Flexible Vehicles: A Liapunov Control Law Design Method," Mechanics and Control of Large Flexible Structures, Progress in Astronautics and Aeronautics, Vol. 129, 1990, PP. 565-593.

Oakley, C.M. and Canon, R.H., "Theory and Experiments in Selecting Mode Shapes for Two-Link Flexible Manipulators," Proceedings of First International Symposium on Experimental Robotics, Montreal, Canada, June 1989.

Singh, S.K., Gran, R., and Agrawal, B.N., "Comparison of Different Attitude Control Schemes for Large Communications Satellites," Proceedings of AIAA Guidance, Navigation, and Control Conference, Monterey, California, August 1987.

Agrawal, B.N., and Watkins Jr., R.J., "Experimental Verification of Attitude Control Techniques for Flexible Spacecraft," 42nd Congress of the International Astronautical Federation, Montreal, Canada, October 5-11, 1991.

Kwakernaak, H., Sivan, R., "Linear Optimal Control Systems," Wiley-Interscience, New York, 1972.